J|A|C|S ARTICLES

Published on Web 04/09/2009

In Situ and Real-Time Monitoring of Oxide Growth in a Few Monolayers at Surfaces of Platinum Nanoparticles in Aqueous Media

Hideto Imai,*,† Koichi Izumi,† Masashi Matsumoto,† Yoshimi Kubo,† Kazuo Kato,‡ and Yasuhiko Imai‡

Nano Electronics Research Laboratories, NEC Corporation, 34 Miyukigaoka, Tsukuba 305-8501, Japan, and Japan Synchrotron Radiation Research Institute, 1-1-1 Kouto, Sayo-cho, Hyogo 679-5198, Japan

Received December 31, 2008; E-mail: h-imai@ce.jp.nec.com

Abstract: The electrochemical oxidation behaviors of the surfaces of platinum nanoparticles, one of the key phenomena in fuel cell developments, were investigated in situ and in real time, via time-resolved hard X-ray diffraction and energy dispersive X-ray absorption spectroscopy. Combining two complementary structural analyses, dynamical and inhomogenous structural changes occurring at the surfaces of nanoparticles were monitored on an atomic level with a time resolution of less than 1 s. After oxidation at 1.4 V vs RHE (reversible hydrogen electrode) in a 0.5 M H_2SO_4 solution, longer Pt−O bonds (2.2−2.3 Å that can be assigned to OHH and/or OH species) were first formed on the surface through the partial oxidation of water molecules. Next, these species turned to shorter Pt−O bonds (2.0 Å, adsorbed atomic oxygen), and atomic oxygen was incorporated into the inner part of the nanoparticles, forming an initial monolayer oxide that had α-PtO_2-like local structures with expanded Pt−Pt bonds (3.1 Å). Finally, quasi-three-dimensional oxides with longer Pt−(O)−Pt bonds (3.5 Å, precursor for β-PtO_2) grew on the surface, at almost 100 s after oxidation. Despite the very complex oxidation mechanism on the atomic level, XANES analysis indicated that the charge transfer from platinum to the adsorbed oxygen species was almost constant and rather small, that is, about 0.5 electrons per oxygen, up to two monolayers of oxygen. This means that ionic polarization hardly develops at this stage of the surface platinum's "oxide" growth.

Introduction

The electrochemical oxidation of metal surfaces, occurring by direct reaction with oxygen or by reactions through water oxidation in aqueous solutions, is one of the most important interfacial processes in surface science, electrocatalysis, and corrosion science. The oxidation behavior at the platinum surface has especially attracted tremendous interest due to its significance for practical applications like increasing catalytic activity and the durability of Pt catalysts in fuel cells.

Although a considerable amount of work has been carried out to understand how surface oxides, including oxygen-containing-intermediate species, are formed on the platinum surface in an aqueous solution and how such surface oxides affect the catalytic activity toward reducing oxygen, direct observations of such oxidation behaviors are very limited, especially of nanoparticles. Details regarding the precise structure of the surface oxides and other intermediate species, the electronic properties of the surfaces, and their kinetics of formation are not well understood.[1−7] This is because there are two major difficulties with in situ observation of electrochemical reactions at nanoparticle surface in aqueous media.

First, experimental methods for monitoring the structure of the surfaces of nanoparticles in an electrochemical environment are severely limited due to the inability of most probes (such as electrons and neutrons) to penetrate the surrounding electrolytes. A possible approach to overcome this difficulty is to use X-rays from a synchrotron radiation source, which have higher brightness and intensity. Unlike electrons or neutrons, synchrotron X-rays (with higher photon energy) can easily penetrate aqueous solutions, allowing us to monitor the structure of catalyst surfaces through surrounding electrolytes and even electrode materials.

Second, because electrochemical reactions of interest usually take place at the surface or within a few monolayers of the surface of catalyst particles, the simple methods of structural analysis that probe the average characteristics of the whole nanoparticles cannot provide information that is specific to the surface. We propose that we can solve this problem by

† NEC Corp.
‡ Japan Synchrotron Radiation Research Institute.

(1) Jerkiewicz, G. In *Interfacial Electrochemistry: Theory, Experiment, and Applications*; Wieckowski, A., Ed.; Marcel Dekker: New York, 1999; pp 559−576.
(2) Markovic, N. M.; Ross, P. N., Jr. In *Interfacial Electrochemistry: Theory, Experiment, and Applications*; Wieckowski, A., Ed.; Marcel Dekker: New York, 1999; pp 821−842.
(3) Vetter, K. J.; Schultze, J. *J. Electroanal. Chem.* **1972**, *34*, 141–158.
(4) Jekiewicz, G.; Vatankhah, G.; Lessard, J.; Soriaga, M. P.; Park, Y.-S. *Electrochim. Acta* **2004**, *49*, 1451–1459.
(5) Alsabet, M.; Grden, M.; Jerkiewicz, G. *J. Electroanal. Chem.* **2006**, *589*, 120–127.
(6) Conway, B. E.; Barnett, B.; Kozlowska, H. A.; Tilak, B. V. *J. Chem. Phys.* **1990**, *93*, 8361–8373.
(7) Nwoko, V. O.; Uhlig, H. H. *J. Electrochem. Soc.* **1965**, *112*, 1181–1185.

combining two different methods of structural analysis that are complementary, X-ray absorption spectroscopy (XAS) and X-ray diffraction (XRD). These techniques are both "X-ray-in" and "X-ray-out" methods of analyzing structures, suitable for in situ measurements and capable of exploring the structure of a wide variety of samples including both crystalline and noncrystalline materials. While XAS yields information on the local structure around the absorbing atoms, XRD provides information on rather longer length scales reflecting the periodic nature of structures. Hence, by combining these two methods, we expect that we will be able to determine inhomogeneous structural changes in catalyst nanoparticles more accurately than with a single method. Local structural changes occurring near the surface could be determined using XAS, while the structure of the core of the particles, which is rather intact having a periodic structure, could mainly be characterized by XRD. Note that, although XAS has been often applied to the in situ and/or time-resolved studies of fuel cell electrocatalysts, and has yielded much helpful information,[8−17] structural changes on the surface have not yet actually been determined, because XAS only yields average information on all of the nanoparticles.

To obtain a complete picture of the surface reactions of nanoparticles, the electronic level information must be combined with the structural details. For example, the solid-state electrochemical (EC)-NMR studies explained the improved CO tolerance in PtRu fuel cell catalysts via quantitative information on the interaction between CO and metals from both metal and ligand local density of states at Fermi level (E_F-LDOS).[18] XAS offers similar electronic structure insights of nanoparticles through the number of d-orbital vacancies evaluated from X-ray absorption near-edge structure (XANES).[19] Absorption intensity for XANES is very sensitive to adsorption of molecules or surface oxidation, which is accompanied by a possible electron transfer from the metal surface, that is, a change in the electron occupancy of the metal d-band.

In the following, we present the experimental results on the direct monitoring of the behaviors of a few monolayers of oxide growth on the surfaces of platinum nanoparticles during their processes of electrochemical oxidation at 1.4 V vs RHE, reversible hydrogen electrode. The dynamical and inhomogeneous oxidation processes at the surfaces of platinum nanoparticles were directly observed by using two different methods of time-resolved structure analysis, time-resolved energy-dispersive X-ray absorption spectroscopy and time-resolved X-ray diffraction with a time resolution of less than 1 s. The results revealed that platinum oxides are formed through OH adsorption and its dehydration to atomic oxygen. Further oxidation is caused by the diffusion of atomic oxygen into the cores of particles, which gives an atomic-level explanation for the "place-exchange" mechanism of oxide growth.

Experimental Section

Catalysts, Electrode, Electrochemical Cell, and Electrochemical Measurements. Highly dispersed carbon-supported platinum nanoparticles (50 wt % Pt-loading) were prepared with a conventional platinum-oxide-colloidal method.[20,21] The average particle size determined by TEM observation (see Figure 1) and line-broadening analysis of X-ray diffraction profiles was ca. 2 nm. The supported platinum nanoparticles were spread onto a thin carbon electrode (thickness, 120 μm; area, ca. 1 cm^2) with a Nafion ionomer. The electrode, with a platinum-gauze counter electrode and an Ag/AgCl reference electrode, was placed in an originally designed three-electrode electrochemical cell. The electrolyte was a 0.5 M H_2SO_4 aqueous solution (see Supporting Information (Figure S1) for details). The thickness of the electrolyte layer was about 0.5 mm, keeping it as thin as possible to prevent the electrolyte from absorbing the X-rays, but maintaining good electrochemical responses. The advantage of our catalyst electrode and the electrochemical cell is that in this configuration, most of our catalysts work effectively (more than 90%),[22] and thus the amount of structural change can be quantitatively evaluated. (Note that the effective catalyst ratio is at most about 30% for standard MEAs.)[23−25]

Prior to the potential step and steady-state oxidation experiments, the surfaces of platinum nanoparticles were electrochemically cleaned by repeating fast cyclic voltammetry (CV) scans in a potential range from 0.0 to 1.0 V. After the CV scans, the potential was kept at 0.4 V, in the double-layer potential region, where the platinum surfaces were free from any adsorbates. Next, the platinum surfaces were oxidized by applying an external potential up to 1.4 V, and both the dynamical and static XRD and XAFS measurements were carried out. This potential range was chosen as corrosion in platinum catalysts could occur in real operating fuel cells at this potential.[26,27]

In Situ and Time-Resolved X-ray Diffraction Measurements. In situ and time-resolved X-ray diffraction (XRD) measurements were carried out at the beamline BL16XU at SPring-8 in a transmission geometry at a photon energy of 30 keV. High intensity hard X-rays with high-penetration capabilities emitted from an undulator source enabled us to observe broad and weak diffraction signals from nanoparticles in an electrolyte, even within very short periods of time (~milliseconds). X-ray diffraction profiles were recorded on a CCD camera with a time resolution of 0.5 s for the time-resolved experiments. In addition to the time-resolved experiments, static-potential measurements in which data were collected

(8) Mukerjee, S.; Srinivasav, S.; Soriaga, M. P.; MacBreen, J. *J. Phys. Chem.* **1995**, *99*, 4577–4589.
(9) Allen, P. G.; Conradson, S. D.; Wilson, M. S.; Gottesfeld, S.; Raistrick, I. D.; Alerio, J.; Lavato, M. *J. Electroanal. Chem.* **1995**, *384*, 99–103.
(10) MacBreen, J.; Mukerjee, S. *J. Electrochem. Soc.* **1995**, *142*, 3399–3404.
(11) Mukerjee, S.; MacBreen, J. *J. Electroanal. Chem.* **1998**, *448*, 163–171.
(12) Russell, A. E.; Rose, A. *Chem. Rev.* **2004**, *104*, 4613–4636.
(13) Mathew, R. J.; Russell, A. E. *Top. Catal.* **2000**, *10*, 231–239.
(14) Rebecca, S. M.; Mathew, R. J.; Russell, A. E. *J. Phys. Chem. B* **2000**, *104*, 1998–2004.
(15) Roth, C.; Benker, N.; Buhrmester, T.; Mazurek, M.; Loster, M.; Fuess, H.; Koningsberger, D.; Ramaker, D. E. *J. Am. Chem. Soc.* **2005**, *127*, 14607–14615.
(16) Allen, P. G.; Conradson, S. D.; Wilson, M. S.; Gottesfeld, S.; Raistrick, I. D.; Valerio, J.; Lovato, M. *Electrochim. Acta* **1994**, *39*, 2415–2418.
(17) Teliska, M.; O'Grady, W. E.; Ramaker, D. E. *J. Phys. Chem. B* **2005**, *109*, 8076–8084.
(18) Tong, Y. Y.; Kim, H.-S.; Babu, P. K.; Waszczuk, P.; Wieckowski, A.; Oldfield, E. *J. Am. Chem. Soc.* **2002**, *124*, 468–473.
(19) Mansour, A. N.; Cook, J. W., Jr.; Sayers, D. E. *J. Phys. Chem.* **1984**, *88*, 2330–2334.
(20) Watanabe, M.; Uchida, M.; Motoo, S. *J. Electroanal. Chem.* **1987**, *229*, 395–406.
(21) Petrow, H. G.; Allen, R. J. U.S. Patent No. 4,044,193, 1977.
(22) Kosaka, M.; Kuroshima, S.; Kobayashi, K.; Sekino, S.; Ichihashi, T.; Nakamura, S.; Yoshitake, T.; Kubo, Y. *J. Phys. Chem. C*, in press.
(23) Xu, H.; Brosha, E. L.; Garzon, F. H.; Uribe, F.; Wilson, M.; Pivovar, B. *Electrochem. Soc. Trans.* **2007**, *11*, 383–391.
(24) Chlistunoff, J.; Uribe, F.; Pivovar, B. *Electrochem. Soc. Trans.* **2006**, *1*, 137.
(25) Aleksandrova, E.; Hiesgen, R.; Eberhard, D.; Friedrich, K. A.; Kaz, T.; Roduner, E. *ChemPhysChem* **2007**, *8*, 519–522.
(26) Ferreira, P. J.; la O', G. J.; Shao-Horn, Y.; Morgan, D.; Makharia, R.; Kocha, S.; Gasteiger, H. A. *J. Electrochem. Soc.* **2005**, *152*, A2256–A2271.
(27) Reiser, C. A.; Bregoli, L.; Patterson, T. W.; Yi, J. S.; Yang, J. D.; Perry, M. L.; Jarvi, T. D. *Electrochem. Solid-State Chem.* **2005**, *8*, A273–A276.

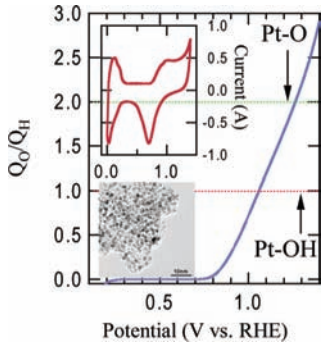

Figure 1. Degree of oxidation as function of potential, estimated by relative oxidation charge to hydrogen absorption charge, assuming successive oxidation reaction. Assuming that active sites are the same for hydrogen adsorption and surface oxidation, oxidation/hydrogen adsorption ratios of 1, 2, and 4 correspond to Pt−OH adsorption, Pt−O adsorption, and nominal PtO_2 formation. The inset shows the cyclic voltammogram of catalyst electrode (electrolyte: 0.5 M H_2SO_4, sweep rate of 5 mV/s).

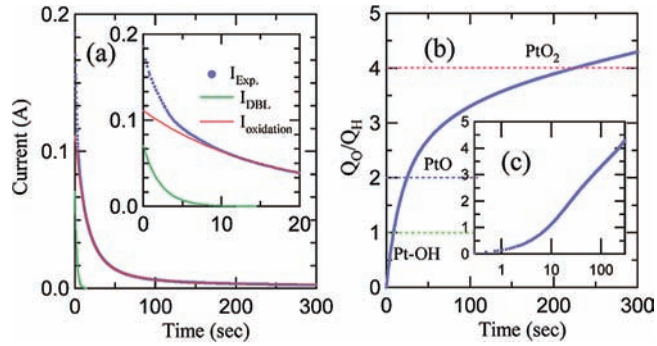

Figure 2. (a) Transient oxidation current at potential step oxidation at 1.4 V vs RHE. Blue dots represent experimental current (I_{EXP}). Green line is electrical double-layer charging current estimated from another potential step experiment in double-layer potential range (I_{DBL}). Red line stands for oxidation current of platinum surface obtained by subtracting I_{DBL} ($I_{oxidation} = I_{EXP} - I_{DBL}$). (b and c) Degree of oxidation during potential step oxidation at 1.4 V vs RHE, as a function of (b) time t and (c) log t. Oxidation ratio is calculated dividing oxidation current by hydrogen absorption current.

using imaging plates with a wider range of diffraction angles were also carried out to cover the limited range of vision and dynamic range of the CCD camera, which only allows us to observe 111- and 220-diffraction peaks. The exposure time for static measurements was about 5 min.

In Situ and Time-Resolved Energy-Dispersive X-ray Absorption Spectroscopy. Time-resolved energy-dispersive X-ray absorption fine structure (DXAFS) spectroscopy measurements were carried out at the beamline BL28B2 (white X-ray beamline) at SPring-8 using the same electrochemical cell.[28] White X-rays emitted from a bending magnet source were diffracted and focused by a curved Si crystal in a polychromator in a Laue configuration with a (111) net plane. The diffracted X-rays had different energies depending on the diffraction angles, covering the energy range for XAS measurements at the Pt L_3 or L_2 edges. All of the absorption spectra were simultaneously acquired by a position sensitive detector, consisting of a scintillator screen coupled to the CCD camera. The spectra were collected every 60 ms, and 15 snapshots were integrated for the XAS analyses. (The actual time resolution was 0.9 s.) In addition to time-resolved DXAFS measurements, conventional step-scanning XAFS measurements on the same samples were also done at the beamline BL16B2 at SPring-8 under static potential control to confirm the results of the structural parameter refinements made in the DXAFS data, which had been obtained in a rather narrow k range.

Results

Electrochemical Responses. We show the electrochemical behaviors of our catalyst electrode in Figures 1 and 2. The inset of Figure 1 shows cyclic voltammograms of the electrode taken in 0.5 M H_2SO_4 solutions. The large background current due to large double-layer capacitance is typical of carbon-supported catalysts with a high surface area. We observed clear hydrogen adsorption and desorption waves that confirmed a good electrochemical response in our catalyst electrode. The degree of oxidation can be estimated from the observed oxidation current as a ratio of oxidation charge, Q_O, and hydrogen adsorption charge, Q_H, assuming successive oxidation reactions, $Pt + H_2O \rightarrow Pt{-}OH + H^+ + e^-$, $Pt{-}OH \rightarrow Pt{-}O + H^+ + e^-$, and $Pt{-}O + H_2O \rightarrow PtO_2 + 2H^+ + 2e^-$ (Figure 1). The onset potential of OH adsorption is around 0.8 V, and at near 1.08 V, the surface is almost fully covered with OH species ($Q_O/Q_H = 1$). Between 1.08 and 1.35 V, the OH species are gradually transformed into Pt−O (adsorbed atomic oxygen) species ($Q_O/Q_H = 2$). At the higher potential, higher order oxides, such as PtO_2, would be formed ($Q_O/Q_H > 2$).

Figure 2a shows the transient current of the potential step oxidation at 1.4 V used for the time-resolved experiments. The degree of oxidation can be roughly estimated as a function of time by integrating oxidation current, similar to the CV measurements. Note, however, that we should carefully treat this transient process, because catalyst electrodes generally have much larger surface areas as well as larger solution/electrode resistance than those of ideal electrodes, and thus they cause a huge electrical double-layer charging current in the potential step experiments. Such double-layer charging current, i_{DBL}, can generally be described as a function of time, t, by

$$i_{DBL} \cong \frac{\Delta E}{R_{sol}} \exp\left(-\frac{t}{R_{sol}C_{dl}}\right)$$

where ΔE represents the potential step magnitude, and R_{sol} and C_{dl} correspond to the solution resistance and the double-layer capacitance.[29] The $R_{sol}C_{dl}$ value of the electrode was determined as 2.26 s by the potential step experiment in the double-layer potential region, from 0.4 to 0.6 V. The C_{dl} value was separately evaluated from the constant term in the CV measurements in the double-layer region as 1.45 F, and then the R_{sol} value was 1.56 Ω. By using these values, the double-layer charging current can be estimated as indicated in Figure 2b by the green line. We then could estimate the degree of oxidation, by integrating the overall oxidation current, $I_{oxidation} = I_{exp} - I_{DBL}$ (Figure 2b). Assuming that the active sites were the same for both the hydrogen adsorption and the oxidation processes, we can see that Pt−OH species was formed in a time range from 0 to 10 s, Pt−O oxidation occurred from 20 to 30 s, and PtO_2 oxidation occurred from 50 to 200 s and beyond. As seen in Figure 2c, we can also see that growth kinetics roughly obeys a direct logarithmic law after 10 s, in our catalyst electrode.[6]

Because of the large time constant of 2.26 s, however, the double-layer charging process takes almost 10 s to be fully charged (90% of charging is completed at ∼5 s, and 99% at ∼10 s). This indicates that the oxidation behavior observed within about 10 s is strongly affected by the electrical double-

(28) Kato, K.; Uruga, T.; Tanida, H.; Yokota, S.; Okumura, K.; Imai, Y.; Irie, T.; Yamakata, Y. *AIP Conf. Proc.* **2007**, *879*, 1214–1217.

(29) Bard, A. J.; Faulkner, L. R. *Electrochemical Method*, 2nd ed.; John Wiley & Sons: New York, 2001; p 15.

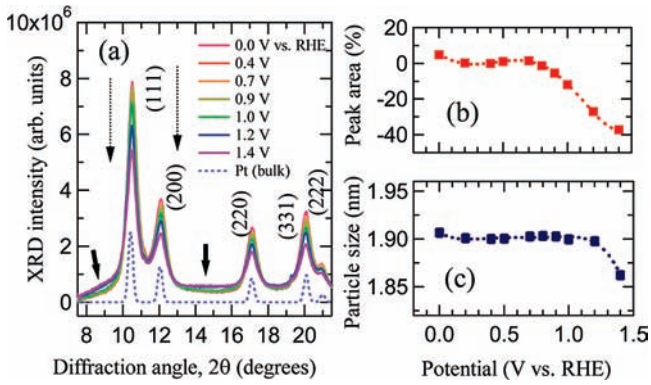

Figure 3. Potential variations in X-ray diffraction profiles for carbon-supported platinum nanoparticles in 0.5 M H_2SO_4. (a), (b), and (c) show potential variations in integrated peak area loss at the 220 peak and the average particle size for core platinum determined by line-broadening analysis with Scherrer's formula.

layer charging and is not a truly intrinsic oxidation process in potential step measurements for the high surface area catalyst electrode. Now, keeping these points in mind, let us look at the effect of potential and time variations on the structural data. Our time-resolved XRD and XAS results offer further details on these processes.

In Situ and Time-Resolved XRD Measurements. During oxidation, the surfaces of platinum nanoparticles are expected to be relaxed or reconstructed by the adsorption of oxygen species (intermediate species of water oxidation such as OH, OHH, and O), and further the surfaces should be covered with their oxides in a higher potential range. Such behaviors can be detected as a reduced intensity in XRD measurements, because the platinum atoms in the relaxed and/or reconstructed parts as well as in the platinum oxides near the surface do not contribute to the diffraction line from "platinum" nanoparticles.

Figure 3a shows the results of in situ XRD measurements, that is, constant potential experiments applying an external potential up to 1.4 V. We can see, as expected, a clear reduction in XRD intensity with increasing potential for all diffraction peaks. Integrated diffraction intensity at the 220 peak gradually decreases above 0.8 V, and finally the fraction of peak area loss reaches 40% (almost the same for all peaks) at 1.4 V, as shown in Figure 3b. For such nanometer-scale particles, the XRD intensity is roughly scaled to the number of atoms that contribute to a certain crystal structure within the framework of kinematic diffraction theory. Hence, the fraction of reduced intensity corresponds to the fraction of platinum atoms in the relaxed or oxide parts that changed from platinum−metal particles. That is, at 0.8 V, the surface of the nanoparticles started to relax with the adsorption of oxygen species, and finally at 1.4 V, almost all of the monolayers of platinum nanoparticles turned to oxides. (Note that the fraction of surface atoms in a 2−3 nm particle is 40−50%.) Above 1.2 V, another broad peak appears as indicated by the increase in background intensity in the 2θ range of about 8−16. This is a direct indication of the formation of surface oxides, which have rather an amorphous structure. (The detailed structure for surface oxides will be discussed later with XAFS data.)

When the surfaces of the nanoparticles are covered with oxides, the core of the metal platinum with an fcc structure would become smaller, causing a line broadening of the XRD peaks. Figure 3c shows the average particle size for the core estimated via analysis of line broadening with Scherrer's formula.[30] Indeed, above 0.9 V, slight line broadening can be observed, indicating that the average diameter of the core particles gradually decreases (from 1.9 to 1.86 Å).

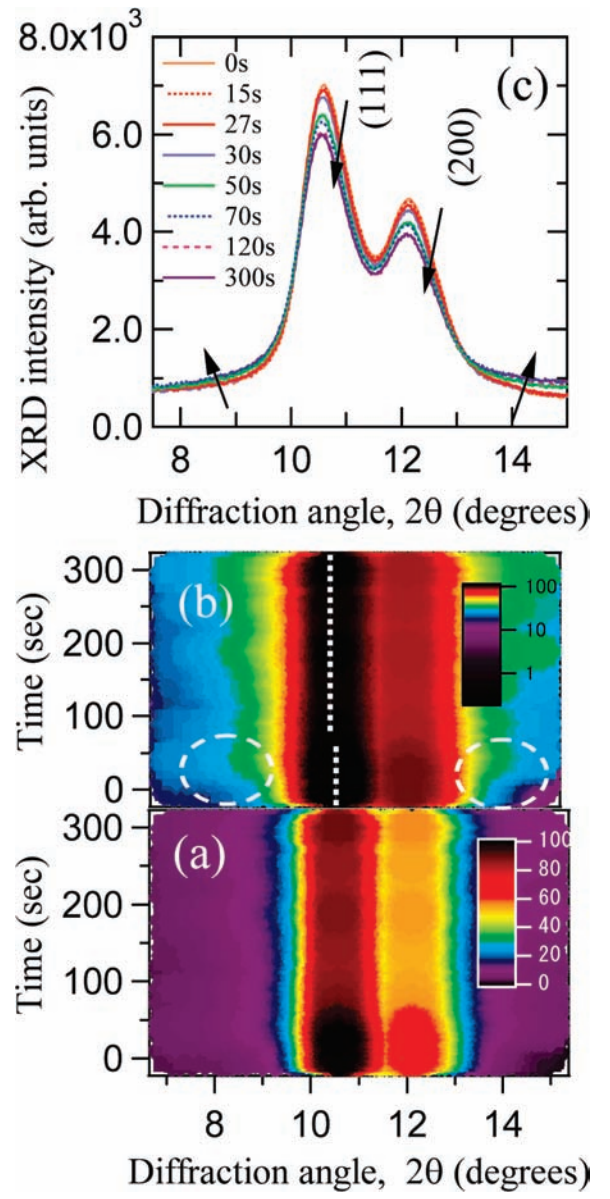

Figure 4. XRD intensity mapped with respect to diffraction angle, 2θ, and time on (a) linear scale and (b) log scale highlighting diffractions from platinum metal nanoparticles and surface platinum oxides, respectively. (c) Time variations of XRD profiles during oxidation at 1.4 V.

These results are consistent with the electrochemical measurements. The observed reduction in intensity beginning at 0.8 V corresponds to the onset of OH adsorption onto the catalyst surface and indicates that OH as well as atomic O adsorption cause lattice relaxation at the catalyst surface. The severely reduced intensity and the increased background intensity observed around 1.2 V could be related to the formation of higher order platinum oxides such as PtO and PtO_2.

Now, let us look into oxidation behaviors in more detail via a potential step oxidation technique using time-resolved XRD measurements. Figure 4a and b displays the XRD intensity

(30) Warren, B. E. *X-ray Diffraction*; Addison-Wesley: Reading, MA, 1968; p 253.

mapped with respect to the diffraction angle, 2θ, and time on (a) a linear scale and (b) a log scale highlighting respective diffractions from platinum metal nanoparticles and surface platinum oxides. Figure 4c shows the XRD profiles with respect to 2θ. The fundamental features are identical to those observed in the constant potential experiments. That is, the oxidation process is characterized by reduced intensity, line broadening, and peak shift.

Within 30 s, the XRD intensities for both 111 and 200 peaks remain almost unchanged, indicating that severe surface roughening does not take place; instead, more incipient oxidation, such as the adsorption of oxygen-containing species, could occur during this period. Near 30 s, platinum oxides begin to form, as indicated by the drastic changes in the time variations of XRD profiles. The XRD intensities for both 111 and 200 peaks rapidly decrease (Figure 4a), while the background intensity that originated from diffuse scattering of amorphous oxides increases (Figure 4b). Simultaneously, the positions of these peaks shift toward lower diffraction angles (increasing lattice constant) with slight line broadening (Figure 4a). The degree of lattice expansion estimated from this peak shift is very small, that is, less than 0.001 Å; nevertheless, this indicates that the core of the platinum metal cluster is totally relaxed when the surface of the nanoparticles is covered with platinum oxides.

From the results of XRD measurements carried out on both static and dynamical oxidation processes, we could conclude that about two monolayers of oxygen atoms are progressively adsorbed on the surface of the platinum nanoparticles at 1.4 V (a monolayer of platinum turned into oxide-like PtO_2), while the core still has an fcc platinum structure with a slightly relaxed form. The oxidation also progresses via two different processes at least, with or without roughening the surface. However, information obtained from XRD measurements that reflect long-range correlation alone is insufficient to discuss the inhomogeneous structural change that mainly occurred at the surface of the nanoparticles. In the following, we will discuss the structure of adsorbates and surface oxides (in addition to the core) as well as their formation kinetics by using extended X-ray absorption fine structure (EXAFS) spectroscopy and X-ray absorption near edge structures (XANES), that is, a local structural probe that enables us to determine the structure around a specific atom as well as the electronic structure for absorbing atoms accurately, even if it does not have a periodic structure.

In Situ Time-Resolved DXAFS Measurements. The time variations in k^3-weighted Fourier transforms (FTs) of Pt-L_3 EXAFS during potential step oxidation are shown in Figure 5. We can see three major features in the oxidation process: a decrease in the FT amplitude for the most pronounced peak near 2.7 Å (corresponding to the first nearest neighbor Pt−Pt bond), in turn, slight increases in the FT amplitudes at around 1.5−2 Å (two kinds of Pt−O bonds), and 3.1 Å (Pt−Pt bond in platinum oxides, Pt−O−Pt). Structural parameters such as coordination numbers (CNs) and interatomic distances (R) obtained by multiple shell fitting in r-space are shown in Figure 6a and b as functions of time.

The behavior of the platinum "lattice" determined by DXAFS is basically similar to those observed in XRD measurements. The Pt−Pt bonds in these nanoparticles just before the potential step oxidation are characterized by the bond length of 2.75 Å and the CN of 9.5. The CN for nanoparticles is generally smaller than that of bulk values, because the fraction of surface atoms, which have smaller CN values, is much larger in nanoparticles. The CN value of 9.5 corresponds to an average particle size of

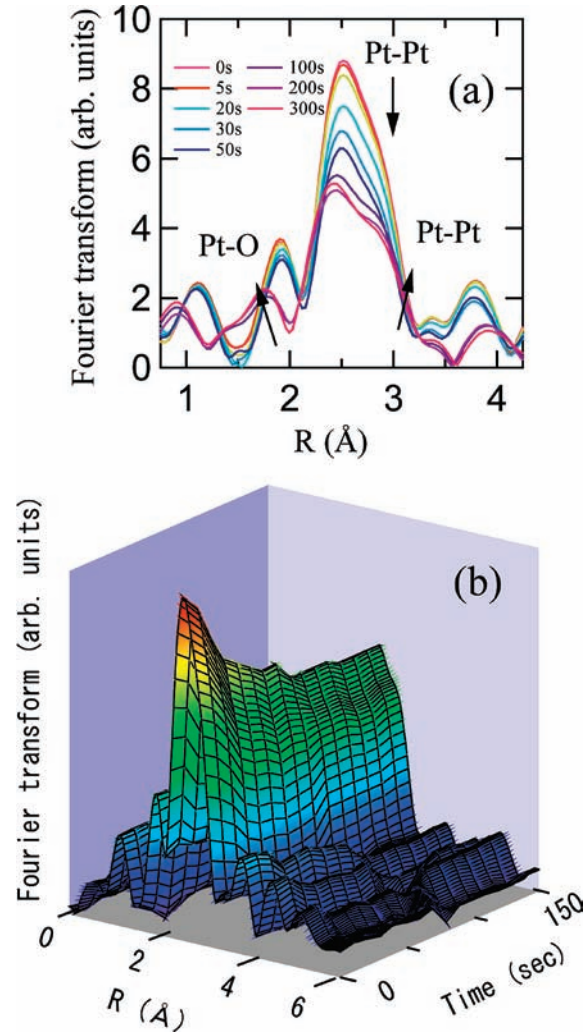

Figure 5. (a and b) Time variations in k^3-weighted Fourier transforms of Pt-L_3 EXAFS during potential step oxidation at 1.4 V. (1) Amplitude of first nearest neighbor Pt−Pt bonds decreases, and in turn (2) amplitude for Pt−O and (3) longer Pt−Pt bonds increase.

ca. 2 nm for platinum metal.[31] After oxidation at 1.4 V, the CN rapidly decreases, and finally reaches 7.8, corresponding to one-layer smaller nanoparticles. Meanwhile, the interatomic distance of Pt−Pt bonds remains almost unchanged. These results are again consistent with the results obtained from time-resolved XRD measurements in that the core of nanoparticles remains almost intact (note that lattice expansion of less than 0.001 Å could not be determined from EXAFS analysis), while the surface is almost completely covered with monolayer platinum oxides.

The detailed structure of adsorbates and/or surface oxides could be determined by analyzing the nature of Pt−O bonds. For platinum oxidation in an aqueous solution, the possible oxygen species are Pt−OHH (adsorbed water molecule), Pt−OH (formed by partial oxidation of water molecule), Pt−O (atomic oxygen adsorption), and Pt−O bonds in surface oxides. According to the experimental reports and the results of theoretical calculations, these Pt−O bonds have slightly different bond lengths, that is, 2.3 Å for Pt−OHH, 2.2 Å for Pt−OH, and 2.0 Å for both adsorbed atomic oxygen

(31) Benfield, R. E. *J. Chem. Soc., Faraday Trans.* **1992**, *88*, 1107–1110.

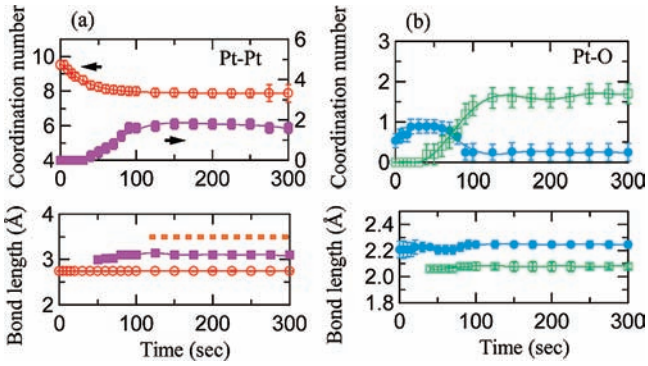

Figure 6. Time variations in bond lengths and coordination numbers for (a) possible Pt−Pt and (b) Pt−O bonds during potential step oxidation at 1.4 V. In addition to Pt−Pt bonds with 2.7 Å (platinum metal), two kinds of longer Pt−Pt bonds (Pt−Pt bonds in platinum oxides, 3.1 and 3.5 Å) appeared at about 40 and 100−120 s, respectively. Longer Pt−O bonds (adsorbed oxygen species) gradually transformed into shorter Pt−O (Pt−O bonds in oxides). See the text for details.

and Pt−O in platinum oxides.[32−36] (Although there are some differences among the reported values, the general trend in bond length is on the same order.)

In EXAFS analysis, we found two kinds of Pt−O bonds with different bond lengths as shown in Figure 6b. The Pt−O bond formed just after oxidation has a bond length of 2.2−2.3 Å, which can be assigned to Pt−OHH and/or Pt−OH. The CN gradually increases, indicating that coverage by such oxygen species is increasing. After about 30−50 s, the CN for the Pt−OH and/or Pt−OHH decreases, and, in turn, another Pt−O bond with a shorter bond length of 2.0 Å appears. This Pt−O bond may be an adsorbed Pt−O (atomic oxygen at surface) or Pt−O bond in the surface oxides. If two- or three- dimensional oxides are formed on the surface, there would be longer Pt−Pt bonds in the oxide lattice such as bridged Pt−Pt in Pt−O−Pt. Indeed, we found longer Pt−Pt bonds (with 3.1 Å) had formed after about 40−50 s after oxidation, and another longer Pt−Pt bond had formed (with 3.5 Å) after 100−120 s as shown in Figure 6a. Hence, the shorter Pt−O bonds observed primarily between 30 and 40 s could be adsorbed atomic oxygen that had formed through the discharge of Pt−OH, while Pt−O bonds found after 40 s could be assigned to Pt−O in two- or three-dimensional oxides, which are formed via the diffusion of atomic oxygen into the platinum lattice.

More insights into the structure of the oxides can be obtained by analyzing the radial distribution function in detail. Figure 7 shows the Fourier transform of Pt L_3-EXAFS obtained at 150 s after oxidation. The dotted line represents a simulated radial distribution function assuming Pt−Pt bonds with 2.75 Å and two kinds of Pt−O bonds with 2.2 and 2.0 Å. There are clear discrepancies around the radials of 3.1 and 3.5 Å, and these would have originated from the surface oxides, that is, Pt−Pt bonds in oxides. We observed Pt−Pt bonds of 3.1 Å at 40 s, and longer Pt−Pt bonds of 3.5 Å appeared after 100−120 s. As listed in Table 1, among the platinum oxides, such as PtO (NaCl-type and tetragonal), α-PtO_2, and β-PtO_2, only β-PtO_2 has Pt−Pt bonds of both 3.1 and 3.5 Å.[36] (Also, see the Supporting Information Figure S2.) Thus, although surface oxides basically have an amorphous structure, our EXAFS analysis suggests that the final structure of surface oxides formed during oxidation at 1.4 V has a local structure similar to that of β-PtO_2. Note that the bond lengths of Pt−O in bulk β-PtO_2 also agree well with those observed in experiments.

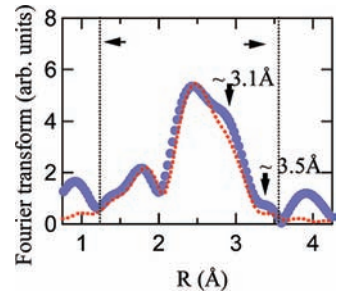

Figure 7. Radial distribution function calculated from the Pt L_3-EXAFS spectrum obtained at 150 s after oxidation. (Blue ●) The red dotted line is a radial distribution function simulated assuming two kinds of adsorbed oxygen species, Pt−OH and Pt−O, that is, Pt−Pt bond (2.77 Å) and two kinds of Pt−O bonds (2.0, 2.2 Å).

Table 1. Bond Lengths of Pt−Pt and Pt−O Bonds in Bulk Platinum Oxides

phase	first NN Pt−Pt	second NN Pt−Pt	first NN Pt−O	second NN Pt−O
PtO	3.040	3.4278	2.023	
PtO	3.6423		2.576	
α-PtO_2	3.100		2.155	
β-PtO_2	3.136	3.5545	1.989	2.0034

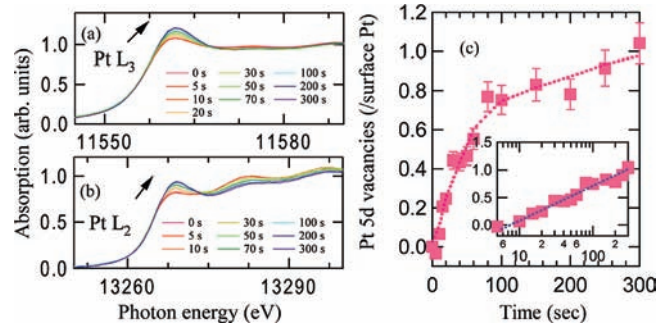

Figure 8. Time variations in XANES spectra during potential step oxidation at 1.4 V vs RHE at Pt (a) L_3 and (b) L_2 absorption edges. (c) Dependence of number of vacancies in platinum 5d orbital on time, per surface platinum atom. The inset shows the number of vacancies platinum 5d orbital with respect to log t.

XANES analyses provided different insight on the reaction mechanism through electronic structural changes caused by surface oxidation. Figure 8a and b shows the time variations in the XANES spectra obtained at both the L_3 and the L_2 absorption edges. As oxidation progressed, we observed a clear increase in white line intensities (i.e., X-ray transition rates) as well as their shifts to a higher energy. This can be attributed to the increase in unoccupied platinum 5d states due to charge transfer from platinum to adsorbed oxygen species. Figure 8c shows the time variations in the number of unoccupied 5d states evaluated by using Mansour's method,[19] simply assuming that electronic alternations only occur at the surface. The number of unoccupied 5d states increased with time and gradually reached a value of about 1.0 vacancy per surface platinum atom at 300 s. The time dependence in Figure 8c looks quite similar to that in Figure 2b. In fact, the increase in platinum

(32) Jacob, T.; Goddard, W. A., III. *J. Am. Chem. Soc.* **2004**, *126*, 9360–9368.
(33) Seitsonen, A. P.; Zhu, Y.; Bedürftig, K.; Over, H. *J. Am. Chem. Soc.* **2001**, *123*, 7347–7351.
(34) Li, T.; Balbuena, P. B. *J. Phys. Chem. B* **2001**, *105*, 9943–9952.
(35) Kumar, J.; Saxena, R. *J. Less-Common Met.* **1989**, *147*, 59–71.
(36) Fernandez, M. P. H.; Chamberland, B. L. *J. Less-Common Met.* **1984**, *99*, 99–105.

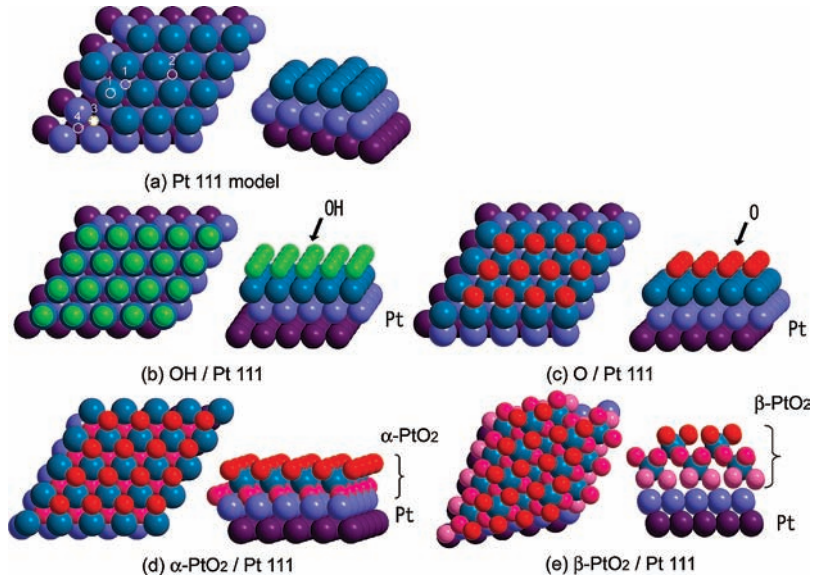

Figure 9. Possible surface-oxidation mechanism drawn on Pt 111 model surface. (a) Pt 111 three-layer model. (1) The hcp hollow sites, (2) fcc hollow sites, (3) octahedral intestinal sites, and (4) tetrahedral interstitial sites. (b) OH (on top site) adsorption. (c) Atomic oxygen adsorption at fcc hollow sites. (d) Monolayer α-PtO_2 on two Pt-layers. (e) Monolayer β-PtO_2 on two Pt-layers. One-half of the Pt atoms in the first oxide layer are lifted toward the surface.

5d vacancies also obeys a direct logarithmic law as shown in the inset of Figure 8c. Such parallel behaviors indicate that the charge transfer from platinum to the adsorbed oxygen species is almost constant, that is, about 0.5 electrons per oxygen atom, irrespective of oxygen coverage. Theoretical studies have predicted that the amount of charge transfer is 0.38 per oxygen atom when atomic oxygen is adsorbed at fcc hollow sites with full coverage (Pt:O = 1:1), and 0.4 for bridge sites.[34] Our preliminary cluster-model calculation derived 0.7 holes for a metastable oxide with Pt:O = 1:2 coverage. These theoretical predictions roughly agree with the observation above. The oxidation rates for our platinum nanoparticles determined with both XAS and electrochemical data were faster than that of a bulk platinum surface, reflecting the difference between the surface states of nanoparticles and bulk.[3] Oxides can be easily grown at the surfaces of the nanoparticles, because there are edge sites at the surfaces, and they are easier to relax than the inner bulk.

Discussion

The possible oxidation scheme obtained from the in situ and time-resolved X-ray structural analyses is summarized in Figure 9a−f for a Pt 111 surface. Our analysis revealed that the place-exchange oxidation mechanism involves two oxidation steps (including α to β-PtO_2 phase transition) that occur after reversible OH and/or atomic O adsorption at solution/metal interface.

The first oxidation step begins with OH adsorption on the surface, which occurred above ∼0.8 V in the steady-state experiments and was completed within the double-layer charging process (∼10 s) in the potential step experiments. The OH species adsorbed an on-top site having a Pt−O bond length of 2.2 Å (Figure 9b). These OH species are further oxidized to atomic oxygen. Atomic oxygen moves to 3-fold hollow sites (fcc- or hcp-hollow sites), forming rather shorter Pt−O bonds with a bond length of 2.0 Å (around 1.0 V or 20−30 s after the potential step). Theoretical studies have also predicted that these 3-fold hollow sites are more stable than on-top sites for O species, although whether fcc or hcp sites are more stable remains a matter of debate. Most oxygen atoms still remain on the surface, and the surface is not severely roughened during these oxidation processes (Figure 9c).

Next, adsorbed oxygen atoms enter the inner part of the platinum lattice by place exchange to form initial two-dimensional oxides (at around 1.2 V, or a time range of around 30−120 s). This behavior was clearly detected by the XRD measurements as a drastic intensity decrease, and also in the EXAFS as the appearance of longer Pt−Pt bond lengths (∼3.1 Å) in addition to the metallic ones (∼2.7 Å). The oxygen atoms would enter the octahedral interstitial sites located just below the fcc hollow site, rather than the narrow tetrahedral ones beneath the hcp hollow site, because of the large atomic radius of oxygen (0.61 Å). Next, the first layer of the Pt 111 surface is slightly lifted by oxygen atoms, making the Pt−Pt bonds longer.

The local Pt−O structure of this phase can be seen as part of the α-PtO_2 (Figure 9d); α-PtO_2 has a layered structure consisting of edge-shared PtO_6 octahedral layers stacked via a van der Waals gap (chemical composition is PtO_2). This PtO_6 octahedral layer can be reproduced by adding oxygen to each hcp hollow site in addition to the octahedral interstitial sites (also see Figure S2a). Note that no longer Pt−Pt bonds of ∼3.5 Å exist in this structure. This is consistent with our experiments; we only observed Pt−Pt bonds with 3.1 Å, and we did not observe any longer Pt−Pt bonds.

Because of the large lattice mismatch of 10% at α-PtO_2-like layer and Pt metal, this α-PtO_2-like layer is unstable and will transform to another quasi-3D structure as more oxygen is adsorbed. We note that even after the place-exchange process (after ∼100 s), we still observed a small number of coexisting OH bonds (∼2.2 Å) (Figure 6). This suggests that OH species can also be adsorbed on new platinum surfaces appearing after place exchange, and they are successively oxidized to form the α-PtO_2-like local structure mentioned above, or they diffuse into the inner regions to promote further oxide growth.

Finally, after about 100−120 s (or near 1.4 V), the quasi-3D oxide begins to form. At this stage of oxidation (more than ∼1.5 monolayers of oxygen), we observed other longer Pt−Pt bonds of ∼3.5 Å, which is a "fingerprint" of β-PtO_2 (also see Figure

9e and Figure S2c). β-PtO_2 consists of PtO_6 octahedra, similar to α-PtO_2, but every other row of the PtO_6 chains is missing in the close-packed layers, and these chains move to the interlayer of the α-PtO_2 structure. This transformation creates longer Pt−(O)−Pt bonds of 3.5 Å. In the β-PtO_2 structure, one-half of the Pt atoms in the initial two-dimensional α-PtO_2-like oxide layer are lifted toward the surface, relaxing the lattice mismatch and forming a quasi-3D oxide layer. Because this structural change from an α-PtO_2-like to a β-PtO_2-like structure is accompanied by a large position change in the platinum or platinum-oxide lattice, it would be a very slow reaction that takes several tens to hundreds of seconds.

To date, the place-exchange phenomenon has been experimentally supported by results of in situ X-ray reflectivity[37] and by in situ STM studies[38] on a platinum single crystal, as a surface roughing after oxidation/reduction cycles. X-ray reflectivity (XRR) measurements performed on Pt 111 single crystal in $HClO_4$ solutions revealed there was a critical oxidation level near 1.25 V, and above this level, the surface is irreversibly roughened, whereas below the critical level, the oxidized surface (Pt atoms is only lifted up) was reversibly reduced to the flat surface. The irreversibly reduced surface (oxidized above 1.25 V) was modeled by an additional layer of Pt atoms over original surface, and this is evidence of the formation of 3D oxides. In comparison with our results, the critical point observed in XRR corresponds to the onset of β-PtO_2 formation, while the reversibly reducible oxide phase observed below the critical level corresponds to α-PtO_2; the monolayer of the platinum surface is lifted by monolayer oxide formation. Because, at the initial stage of oxide formation (up to ∼1.5 monolayers of oxygen), the expansion in the Pt lattice is as large as 10%, oxide growth (α-PtO_2) begins relatively epitaxially, for example, by oxygen being inserted into the octahedral site of the fcc Pt lattice, and thus is reducible to the flat surface. In situ STM observations also indicated irreversible oxidation due to 3D oxide formation. After repeating potential cycles between 0.05 and 1.5 V, the severely roughed surface, that is, island structure with three atomic layers, was observed. These results agree well with our result of β-PtO_2 formation. Our in situ and time-resolved studies have deepened the understanding of the place-exchange mechanism, identifying the local structure of the oxides by directly determining of the nature of Pt−O bonds in real time during oxidation.

A striking observation in the present study was that the charge transfer from Pt to the adsorbed oxygen species determined by XANES was almost constant and unusually small, that is, ∼0.5 electrons per oxygen, up to two monolayers of oxygen (i.e., the formation of a PtO_2 monolayer). These results demonstrate that the nature of the PtO_2 monolayer is very different from that of bulk oxides consisting of Pt^{4+} (or Pt^{2+}) and O^{2-} ions. Little ionic polarization occurs at this stage of surface oxidation. Indeed, the formation of the PtO_2 monolayer seems to be only the successive process for oxygen chemisorption, although it involves some rearrangements of Pt atoms, without developing any further ionicity.

Conclusion

In conclusion, we demonstrated that inhomogeneous structural changes occurring at the surfaces of nanoparticles, that is, the process of forming a few monolayers of oxide on the surfaces of platinum nanoparticles in aqueous H_2SO_4 solution, could be monitored in situ and in real time by combining two complementary methods of structure characterization using synchrotron X-rays, in situ and time-resolved X-ray diffraction and X-ray absorption spectroscopy. When the nanoparticle surface was oxidized at 1.4 V vs RHE, a few monolayers of platinum at the surfaces of the nanoparticles were transformed into amorphous platinum oxides. The intermediate oxygen species as well as the local structures of theses oxides were determined from the lengths of Pt−O bonds. At the initial stage of oxidation, during the electrical double-layer charging process (within ∼10 s), OHH/OH species, which have a Pt−O bond length of 2.2−2.3 Å, were adsorbed on the platinum surface. Next, the double layer was fully charged, the surface OH species were oxidized into atomic oxygen with a Pt−O bond length of 2.0 Å (20−30 s), and atomic oxygen entered the inner portion of the nanoparticles, forming α-PtO_2-like 2D oxides with an expanded Pt−Pt bond length of 3.1 Å (30−120 s, up to ∼1.5 monolayers of oxygen). Finally, the quasi-3D platinum oxide with a β-PtO_2-like local structure (with Pt−Pt of 3.5 Å), which seemed to be more stable than the α-PtO_2-like structure, was formed (120−300 s, more than ∼1.5 monolayers of oxygen). The OH species were continuously adsorbed on the new surface formed after place exchange, providing oxygen atoms to the metal/oxide interface. During these oxidation processes, the core of the platinum particles was almost intact, but it had a slightly relaxed structure. XANES analysis revealed that the charge transfer from Pt to the adsorbed oxygen species was almost constant and small, that is, ∼0.5 electrons per oxygen atom, up to two monolayers of oxygen. This meant that little ionic polarization developed in the PtO_2 monolayer "oxide".

Acknowledgment. The synchrotron radiation experiments were performed at SPring-8 with the approval of the Japan Synchrotron Radiation Research Institute (JASRI) (proposal nos. J04B28B2-0518N, C04B16XU-4080N, C04B16B2-4080N, C05A16XU-4080N, C05A16B2-4080N, 2005A0263NI-np, 2005B0847, 2006A0126, 2005B5080, 2005B5380, 2006A5080, and 2006A5380). We thank Dr. T. Ichihashi for the TEM observation of the carbon-supported platinum nanoparticles.

Supporting Information Available: Electrochemical cell designed for in situ synchrotron X-ray measurements; and crystal structure of bulk platinum oxides. This material is available free of charge via the Internet at http://pubs.acs.org.

JA810036H

(37) You, H.; Zurawski, D. J.; Nagy, Z.; Yonco, R. M. *J. Chem. Phys.* **1994**, *100*, 4699–4702.
(38) Itaya, K.; Sugawara, S.; Sashikata, K.; Furuya, N. *J. Vac. Sci. Thechnol., A* **1990**, *8*, 515.